atoms

MDPI

Article

Cross Sections and Rate Coefficients for Vibrational Excitation of HeH^+ Molecule by Electron Impact

Mehdi Ayouz [1,†] and Viatcheslav Kokoouline [2,*,†]

[1] Laboratoire de Genie des Procedes et des Materiaux, Ecole Centrale Paris, CentraleSupelec, campus de Chatenay-Malabry Grande Voie des Vignes F-92 295 Chatenay-Malabry Cedex, France; mehdi.ayouz@centralesupelec.fr

[2] Department of Physics, University of Central Florida, Orlando, FL 32816, USA

* Correspondence: viatcheslav.kokoouline@ucf.edu; Tel.: +1-407-823-5145

† These authors contributed equally to this work.

Academic Editor: Bastiaan J. Braams

Received: 11 November 2016; Accepted: 14 December 2016; Published: 20 December 2016

Abstract: Cross sections and thermally-averaged rate coefficients for vibration (de-)excitation of HeH^+ by an electron impact are computed using a theoretical approach that combines the multi-channel quantum defect theory and the UK R-matrix code. Fitting formulas with a few numerical parameters are derived for the obtained rate coefficients. The interval of applicability of the formulas is from 40 to 10,000 K.

Keywords: helium hydride ion; vibrational excitation; R-matrix; quantum-defect theory

1. Introduction

The hydrohelium (helium hydride) cation HeH^+ is an important species in the interstellar medium (ISM) [1] and in the chemistry of the planetary nebulae such as NGC 7027 [2–4]. It is one of the simplest molecular ions and the first one formed in the early universe [5]. In the ISM it is formed mainly in the process of radiative association of He and H^+ or of He^+ and H [6,7]. Due to the relatively large abundance of electrons and HeH^+ in the ISM, collisions of HeH^+ with electrons play a significant role, in particular, leading to dissociation (dissociative recombination) and rovibrational (de-)excitation of HeH^+. Other than in the ISM, the HeH^+ ion is also present in fusion reactors. Because it is one of the most abundant molecular ions near walls of the reactors, its contribution to the complete network of processes taking place in the reactors should be accounted for in fusion plasma modeling. In particular, cross sections for electron-HeH^+ collisions are needed.

A number of processes can occur when an electron collides with HeH^+. One of the most important processes is the dissociative recombination. Cross sections for this process were measured and calculated in several previous studies [8–13]. Another process, relevant for the ISM [14] and fusion reactors, in the vibrational excitation and (de)-excitation,

$$e^- + \mathrm{HeH}^+(v,j) \rightarrow e^- + \mathrm{HeH}^+(v',j')\,, \tag{1}$$

for which cross sections were calculated in a previous study [15] for the transitions between the three lowest vibrational levels $v = 0, 1, 2$. In that study, an R-matrix approach was employed to determine scattering matrices for fixed geometries. Rydberg series of vibrational and rotational resonances present in the spectrum of the $e^- - \mathrm{HeH}^+$ system were neglected. In this work we determine cross sections and rate coefficients for the process using an improved treatment, in which the Rydberg series of vibrational resonances in HeH are accounted for using the multichannel quantum defect theory (MQDT). Electron-impact transitions between the five lowest vibrational levels, $v = 0 - 4$, are considered.

The rest of the article is organized in the following way. The next section of the article discusses the theoretical approach used in the present calculation. In Section 3, the obtained rate coefficients for vibrational (de-)excitation are discussed and compared with the data available in literature. Section 4 concludes the study.

2. Theoretical Approach

2.1. Scattering Matrix for Fixed Geometries Of HeH^+

The theoretical model employed in the present study combines the UK R -matrix method [16,17] and the multi-channel quantum defect theory (MQDT) [18–20]. The electron scattering calculations were performed employing the Quantemol-N interface [21] to run the UK R-Matrix code [16,17]. The target HeH^+ ion was assumed to be in the ground electronic state $X^1\Sigma^+$.

In the R-matrix calculations, the target and the scattering wave functions were represented within a full CI treatment, i.e., by allowing all electrons to occupy all orbitals. The calculations were performed using the Gaussian basis set 6-311G*. The continuum orbitals of Faure et al. [22], representing the scattering electron, was included up to the g-wave. The R-matrix radius was set to $a_0 = 10$ bohrs. All generated states up to 25 eV were retained in the final close-coupling calculation. As the first electronically excited state, $A^1\Sigma^+$ correlated with H(1s) + $He^+(1s)$ is approximately 11 eV above the H^+ + He($1s^2$) dissociation limit for the $X^1\Sigma^+$ground state, the ground state is essentially isolated and non-adiabatic effects are expected to be small. Therefore, for low electron energy collisions (bellow 10 eV) only the lowest electronic state is open for ionization in $e^- - HeH^+$ collisions and the dimension of the geometry-fixed scattering matrix does not change with energy.

Wave functions of $e^- - HeH^+$ continuum states obtained in the R-matrix calculations have the following asymptotic behavior at large distances r between the electron and the target ion in channels open for ionization [16]

$$F_{ij}(r) \sim \frac{1}{\sqrt{k_i}} \left(\sin\theta_i(r)\delta_{ij} + \cos\theta_i(r) K_{ij}(R) \right) , \tag{2}$$

$$\theta_i(r) = k_i r - \frac{l_i \pi}{2} + \frac{\ln(2k_i r)}{k_i} + \arg\Gamma\left(l + 1 - \frac{i}{\pi}\right) , \tag{3}$$

where index i refers to the entrance channel before a collision and j refers to the outgoing channel after the collision. In the above equation, $K_{ij}(R)$ are the elements of the reactance matrix [16,20], which depend on the internuclear distance R. In the cross section calculation, the scattering matrix $\mathbf{S}(R)$ is needed, which is obtained from $\mathbf{K}(R)$ as

$$\mathbf{S}(R) = (\mathbf{1} + i\mathbf{K}(R))(\mathbf{1} - i\mathbf{K}(R))^{-1} . \tag{4}$$

Generally, for fixed geometries of the target and low collisional velocities, the matrices $\mathbf{S}(R)$ and $\mathbf{K}(R)$ depend weakly on energy. A sharper energy-dependence is observed only at certain higher energies, corresponding to positions of Rydberg states attached to excited electronic states of the ion. A convenient way to represent a weak or a strong energy dependence of the matrices is the eigenphase sum. Figure 1 shows eigenphase sums for three symmetries ($^2\Sigma^+$, $^2\Pi$, and $^2\Delta$) of the e^- + HeH^+ system and for several internuclear distances in HeH^+. The chosen interval of internuclear distances corresponds to the Franck-Condon region of the lowest vibrational level of HeH^+. The variation of the eigenphase sums for $^2\Pi$ and $^2\Delta$ is smooth for energies below 10 eV and does not change significantly with R. The $^2\Sigma^+$ eigenphase sums demonstrate a sharp energy dependence at certain energies, which corresponds to a resonant state of HeH with energy changing with the internuclear distance R.

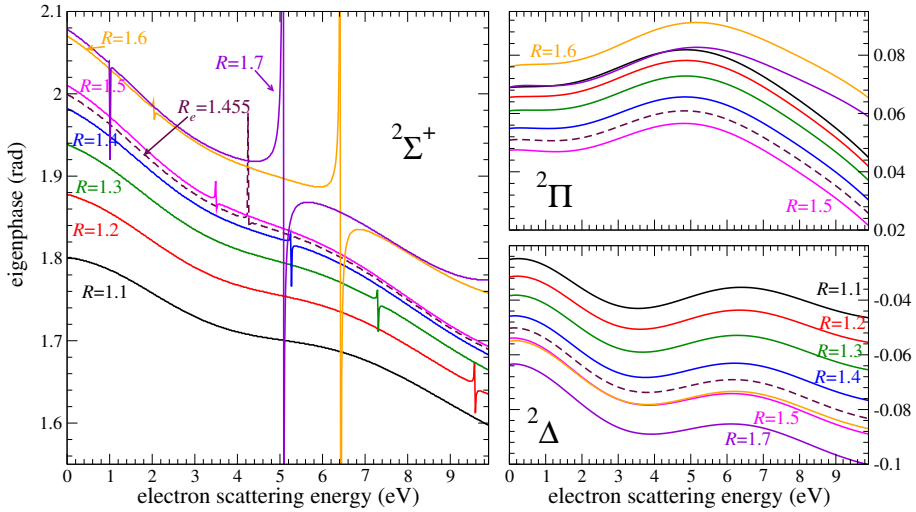

Figure 1. Eigenphase sum as a function of the electron scattering energy E_{el} (in eV) for several internuclear distances R (in units of bohr) for the $^2\Sigma^+$ (left panel), $^2\Pi$ (right upper panel), and $^2\Delta$ (right bottom panel) symmetries. The color scheme used to label different values of R is the same for all three panels. The dashed line represents the equilibrium internuclear distance $R_e = 1.445$ bohrs [15] of HeH^+.

2.2. HeH^+ Vibrational Dynamics

In calculations of the cross section for vibration (de-)excitations, vibrational wave functions of the target ion are needed in order to construct elements of the scattering matrix for transitions from one state v' to another v. We calculated vibrational wave functions $\psi_v(R)$ and energies ϵ_v by solving the Schrödinger equation for vibrational motion along R,

$$\left[-\frac{1}{2\mu}\frac{\partial^2}{\partial R^2} + V(R)\right]\psi_v(R) = \epsilon_v\psi_v(R)\,, \tag{5}$$

where μ the reduced mass and $V(R)$ is the internal potential of HeH^+. The above equation was solved using a DVR-type method [23]. In the numerical calculation, the distance R was varied from 0.5 to 20 bohrs. The potential energy curve $V(R)$ was calculated with the *ab initio* CCSD(T) method and the cc-pVQZ basis of Gaussian-type orbitals using the Molpro package [24]. Figure 2 shows the potential energy curve $V(R)$ and wave functions for four vibrational levels $v = 0, 1, 2, 8$. Energy differences for transitions $v \to v+1$ and rotational constants of the HeH^+ vibrational levels are listed in Table 1 and compared with previous benchmark calculations [25,26].

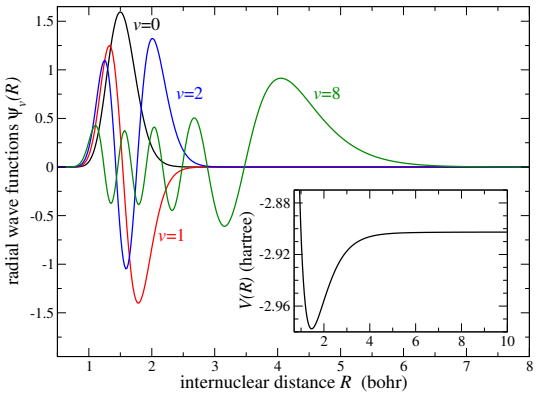

Figure 2. Wave functions $\psi_v(R)$ of the $v = 0, 1, 2$, and 8 vibrational states of the HeH^+ ion. The inset shows the potential energy curve $V(R)$ of the $X^2\Sigma^+$ electronic state of HeH^+ used in the calculation.

Table 1. The vibrational frequencies $\Delta_v = E_{v+1} - E_v$ for transitions $v \rightarrow v+1$ and rotational constants B_v obtained in the present study and compared with previous calculations. All values are in cm^{-1}.

Level v	Δ_v	Δ_v [26]	B_v	B_v [25]
0	2913	2911.0007	33.527	33.558
1	2607	2604.1676	30.816	30.839
2	2300	2295.5787	28.088	28.090
3	1988	1982.0562	25.305	25.301
4	1668	1660.3559	22.425	22.402
5	1339	1327.7860	19.394	19.344
6	1000	984.3599	16.151	16.058
7	660	639.1959	12.645	12.479
8	328	327.3615	8.813	8.621

2.3. The Scattering Matrix for an Electron Colliding with HeH^+

Once vibrational energies, wave functions, and geometry-fixed S-matrix are calculated, the scattering matrix describing the transition amplitude $S_{i',i}$ from one vibrational level v to another v' is obtained using the method of vibrational frame transformation [19,27]. The indexes i' and i enumerate vibrational states v, states of different electron angular momentum l, and its projections Λ on the molecular axis Z. Therefore, for the process

$$e^-(l,\Lambda) + \mathrm{HeH}^+(v) \longrightarrow e^-(l',\Lambda') + \mathrm{HeH}^+(v')\,, \tag{6}$$

the scattering matrix in the molecular frame coordinate system can be written as

$$\mathcal{S}_{\Lambda' v' l',\Lambda v l} = \left\langle \psi_{v'}(R) \left| S_{\Lambda' l',\Lambda l}(R) \right| \psi_v(R) \right\rangle\,, \tag{7}$$

where the brackets imply an integration over the vibrational coordinates. Many elements among $S_{\Lambda' v' l',\Lambda v l}$ are zero. In particular, the symmetry (one of the irreducible representations Γ of the $C_{\infty v}$ group) of the total e^- + HeH^+ system stays the same before and after a collision. Also, for low energies when there is only one electronic state $X^1\Sigma^+$ open for ionization, the $\mathcal{S}_{\Lambda' v' l',\Lambda v l}$ matrix is diagonal over Λ. Note that the matrix element $S_{\Lambda' l',\Lambda l}(R)$ in the above equation is obtained from R-matrix calculations for a given value of R. It represents the scattering amplitude when the electron scatters from one channel (Λl) to another $(\Lambda' l')$, while the nuclei do not have time to move. To evaluate the integral in Equation (7) the R-matrix calculations were performed for thirty values of R in the interval R = 1.0–3.9 bohrs with a step of 0.1 bohrs.

2.4. Elimination of Channels Closed for Ionization From the Scattering Matrix

The scattering matrix $\mathcal{S}$ of Equation (7) can be used for cross sections calculations only if the total energy of the system is high enough for all collision channels to be open for ionization. When some channels are closed, the scattering matrix should be modified applying the "closed-channel-elimination" procedure [20] and producing matrix $\mathcal{S}^{phys}(E)$ according to

$$\mathcal{S}^{phys}(E) = \mathcal{S}^{oo} - \mathcal{S}^{oc}\left[\mathcal{S}^{cc} - e^{-2i\beta(E)}\right]^{-1}\mathcal{S}^{co}\,. \tag{8}$$

The matrix $\mathcal{S}^{phys}(E)$ has $N_o \times N_o$ dimension, N_o being the number of channels open for ionization for a given total energy E of the system. The total energy could be written as a sum of the energy of the entrance channel E_i and the relative kinetic energy E_{el} of electron and the target ion: $E = E_i + E_{el}$. In the above equation, the matrices $\mathcal{S}^{oo}$, $\mathcal{S}^{oc}$, $\mathcal{S}^{cc}$ and $\mathcal{S}^{co}$are submatrices of the original matrix $\mathcal{S}$ [18,20], partitioned as

$$\mathcal{S} = \begin{pmatrix} \mathcal{S}^{oo} & \mathcal{S}^{oc} \\ \mathcal{S}^{co} & \mathcal{S}^{cc} \end{pmatrix}\,, \tag{9}$$

where the partition of the matrix elements in the "o"- and "c"-parts is made on the basis whether the corresponding channel, i or i', is open or closed for ionization for a given total energy E. The quantity $\beta(E)$ is a diagonal $N_c \times N_c$ matrix

$$\beta_{i'i}(E) = \frac{\pi}{\sqrt{2(E_i - E)}}\delta_{i'i}\,, \tag{10}$$

where E_i refers to energy of the corresponding closed channel i and $N_c = N - N_o$ is the number of closed channels. For a given vibrational quantum number v, channel energies are degenerate with respect to l and Λ. In principle, the channel energy E_i depends also on the electronic excitation of the target ion, but in this study the initial electronic state is $X^1\Sigma^+$ and collisional energies are too low to excite other electronic states.

3. Rate Coefficients and Cross Sections for Vibrational (De-)Excitation

Using the scattering matrix $\mathcal{S}^{phys}$, the cross section for electron-impact vibrational transition $v \to v'$ of the ion is [28]

$$\sigma_{v'v}(E_{el}) = \frac{\pi\hbar^2}{2m_e E_{el}} \sum_{\Lambda' l' \Lambda l} \left| \mathcal{S}^{phys}_{\Lambda' l' v', \Lambda l v} - \delta_{\Lambda l v, \Lambda' l' v'} \right|^2 , \tag{11}$$

where m_e is the reduced mass of the electron and the HeH^+ ion. It is also convenient to represent the cross section in the form

$$\sigma_{v'v}(E_{el}) = \frac{\pi}{k_{el}^2} P_{v'v}(E_{el})\,, \tag{12}$$

where k_{el} is the wave vector of the incident electron and $P_{v'v}(E_{el})$ could be viewed as the probability for vibrational (de-)excitation at collision energy E_{el}.

Figures 3 and 4 demonstrate, as examples, the cross sections of Equation (11) and the corresponding probabilities from Equation (12) for the $v = 3 \to v' = 0, 1, 2, 4$ transitions. At very low scattering energies, below 0.02 eV, the de-excitation cross sections are smooth functions inversely proportional to the incident energy of the electron as predicted by the Wigner threshold law. But at higher energies, especially, just below the energy of the each excited threshold, $v' = 4, 5, \cdots$, the (de-)excitation cross sections and probabilities demonstrate series of Rydberg resonances, where they vary significantly.

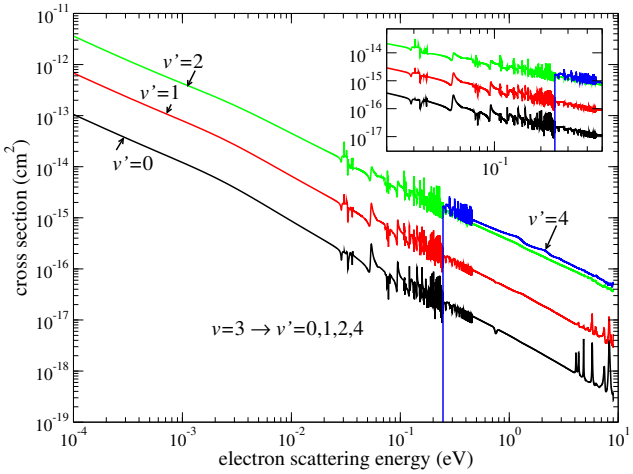

Figure 3. Cross sections of vibrational (de-)excitation from the vibrational level $v = 3$ to several other levels v'. The inset enlarges the region of Rydberg series of resonances close to the $v' = 4$ and $v' = 5$ ionization thresholds, situated at energy of 0.2465 and 0.4533 eV, respectively, above the $v = 3$ threshold.

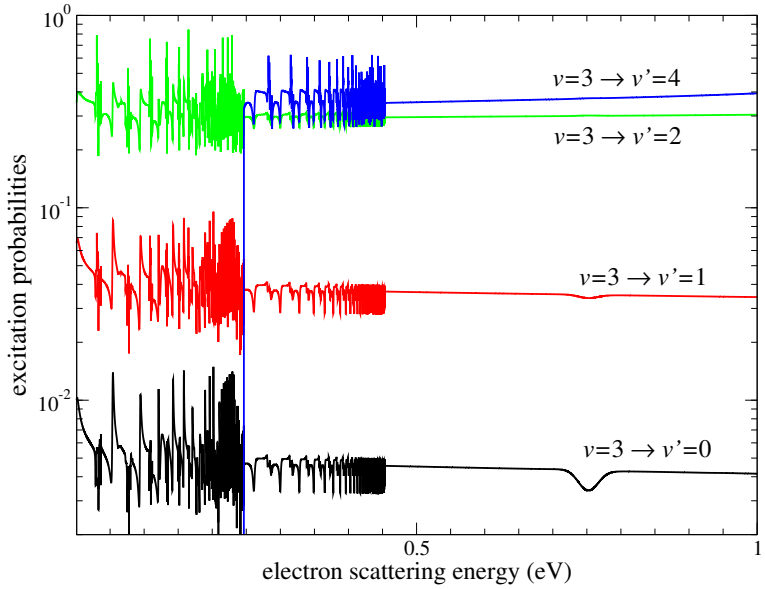

Figure 4. Probabilities $P_{v'v}(E_{el})$ for vibrational (de-)excitation from the vibrational level $v = 3$ to the $v' = 0, 1, 2, 4$ vibrational levels. Notice that the energy scale is linear in contrast to the logarithmic scale in Figure 3.

The thermally averaged rate coefficient $\alpha_{v' \leftarrow v}(T)$ (in atomic units) is obtained from the energy-dependent cross section of Equation (11),

$$\alpha_{v'v}(T) = \frac{8\pi}{(2\pi k_b T)^{3/2}} \int_0^\infty \sigma_{v'v}(E_{el}) e^{-\frac{E_{el}}{k_b T}} E_{el} dE_{el} \,, \tag{13}$$

where k_b is the Boltzmann coefficient and T is the temperature. Examples of obtained rate coefficients $\alpha_{v' \leftarrow v}(T)$ are shown in Figure 5.

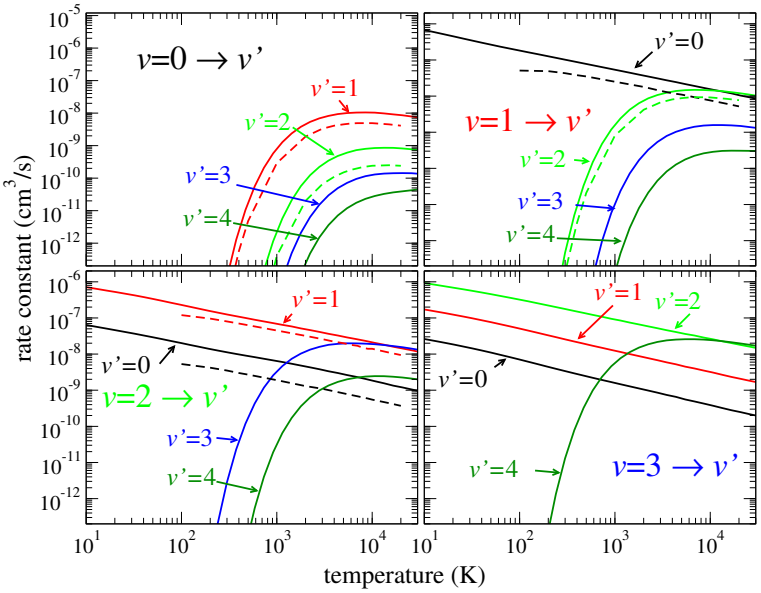

Figure 5. Thermally averaged rate coefficients for several (de-)excitation transitions obtained by direct integration using Equation (13). Vibrational transition $v \rightarrow v'$ labels are shown in each panel. Results of a previous calculation [15] are shown by dashed lines.

In order to simplify eventual applications of the calculated numerical coefficients $\alpha_{v'v}(T)$, the obtained numerical rate coefficients were fitted using the following analytical interpolation formula

$$\alpha^{fit}_{v'\leftarrow v}(T) = \frac{1}{\sqrt{T}} e^{-\frac{\Delta_{v'v}}{T}} P^{fit}_{v'v}(x), \tag{14}$$

where

$$P^{fit}_{v'v}(x) = a_0 + a_1 x + a_2 x^2 + a_3 x^3 \qquad \text{and} \qquad x = \ln(T). \tag{15}$$

with $P^{fit}_{v'v}(x) \approx P^{fit}_{vv'}(x)$. In equation (14), $\Delta_{v'v}$ is the threshold energy having the following expression:

$$\Delta_{v'v} = \begin{cases} E_{v'} - E_v > 0 & \text{for excitation}, \\ 0 & \text{for (de-)excitation}. \end{cases} \tag{16}$$

The coefficients a_i ($i = 0, 1, 2, 3$) are obtained for each pair of transitions $v' \leftrightarrow v$ from a numerical fit. The quantity $P^{fit}_{v'v}(x)$ in the above equation could be viewed as an averaged (de-)excitation probability that varies weakly with energy.

Figure 6 illustrates the rates coefficients for the $v = 3 \rightarrow v' = 0, 1, 2, 4$ transitions obtained numerically from Equation (13) and by the fit of Equation (14). Overall, the fitting curves agree well with the curves obtained numerically. The numerical values of a_i listed in the Table 2 are such that, when plugged into Equation (14), they give rate coefficients in units of $\mathrm{cm}^3 \cdot \mathrm{s}^{-1}$. The temperature in the fitting formulas of Equation (15) is in kelvin.

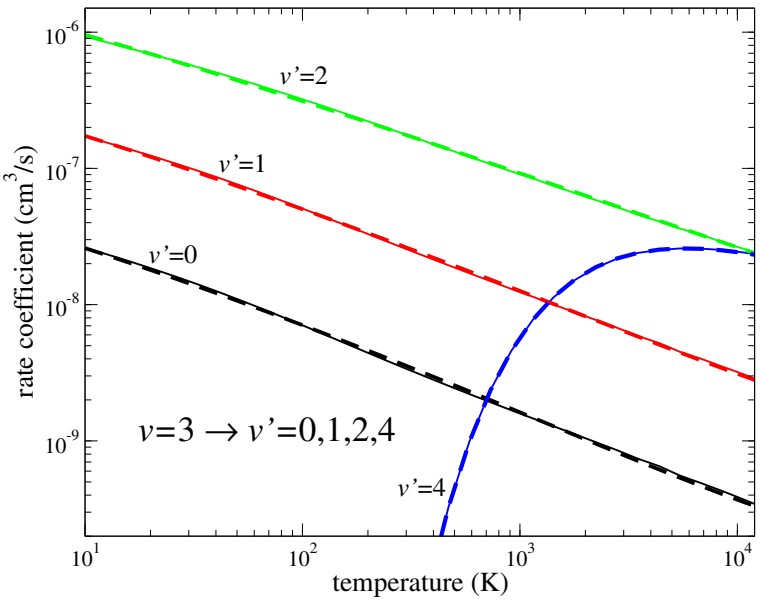

Figure 6. The figure demonstrates the quality of the fit of Equation (14): Numerical and fitted values are shown by solid and dashed lines respectively.

Table 2. Parameters a_0, a_1, a_2 and a_3 of the polynomial $P^{fit}_{v'v}(x) = P^{fit}_{vv'}(x)$ of Equation (14) for several pairs of initial and final vibrational level. The upper line in the header of the table specifies the pairs of initial and final vibrational levels for which the parameters are fitted. For convenience, we also specify (the second line of the header) the threshold energy $\Delta_{v'v}$ for excitation process of the corresponding pair. For all excitation and de-excitation processes, same parameters a_i are used in Equations (14) and (15) where the threshold for de-excitation is zero, $\Delta_{v'v} = 0$, as in Equation (16).

$v' - v$	0–1	0–2	0–3	0–4	1–2	1–3	1–4	2–3	2–4	3–4
$\Delta_{v'v}$ (K)	4191	7942	11251	14112	3751	7060	9920	3309	6169	2860
a_0	0.23e-5	0.20e-6	0.75e-7	0.11e-7	0.21e-5	0.47e-6	0.80e-7	0.24e-5	0.44e-6	0.28e-5
a_1	−0.11e-6	−0.20e-8	0.88e-8	0.31e-9	0.95e-7	0.62e-7	−0.71e-9	0.34e-6	−0.53e-8	0.16e-8
a_2	0.25e-8	0.10e-8	−0.28e-8	−0.24e-10	−0.18e-7	−0.16e-7	0.76e-9	−0.56e-7	0.40e-8	0.13e-7
a_3	0.85e-10	−0.11e-9	0.15e-9	−0.56e-12	0.79e-9	0.85e-9	−0.76e-10	0.22e-8	−0.36e-9	−0.92e-9

4. Conclusions and Discussion

In this study, cross sections and rate coefficients for electron-impact vibrational transitions in HeH^+ were computed for different combinations of the five lowest vibrational levels of HeH^+. The calculations were performed using the UK R-matrix package combined to the quantum-defect approach. The obtained thermally averaged rate coefficients were fitted with a simple analytical formula with four parameters. The numerical values of the fitting parameters are provided in Table 2. The obtained cross sections and rate coefficients could be used in modeling the hydrogen/helium plasma experiments as well as for modeling interstellar clouds and planetary atmospheres, where the HeH^+ ion is present.

The rotational structure of each vibrational level was neglected in the present approach such that the obtained cross sections and rate coefficients should be viewed as averaged over initial rotational states and summed over final rotational states of corresponding vibrational levels. Neglecting the rotational structure would correspond to an experiment for which the energy resolution is worse than a typical energy splitting between rotational levels. The rotational constants for the lowest vibrational levels of HeH^+ are in the interval 20–33 cm^{-1} (see Table 1). The energy resolution of existing experimental data on e^- + HeH^+ collisions is much worse [9]. Detailed rotational state-to-state thermally-averaged rate coefficients for rotational transitions without changing the vibrational state might be useful to model very cold environment, below 40 K. Due to this reason the rate coefficients obtained in the present study should not be viewed as accurate below 40 K. Theoretical rate coefficients for rotational excitation at low temperatures will be presented in a separate study.

It is worth stressing that narrow electronic resonances present in the $e - HeH^+$ spectrum (see Figure 1), around 1 eV and above, are taken into account only in a very crude manner. Namely, they produce scattering matrix $S(R)$ of Equation (4), which depends significantly on energy. Because the resonances are situated at relatively high energies and their widths are small (see, for example, the resonance at 4 eV for $R = 1.455$ bohrs in Figure 1), their effect is expected to be small on the obtained cross sections at low energies. The reason why the effect of such resonances is accounted for in a crude manner is because after the vibrational frame transformation of Equation (7), the resonances will be smeared out and will no appear in the excitation cross section. In a better treatment such resonances associated with HeH^* potential curves should be represented by one or several additional vibronic channels and would produce a few more additional resonances in the cross section for vibrational excitation. In the present treatment, the energy-dependence of $S(R)$, increases the excitation cross section near the corresponding energies but only on average, in a washed-out manner, without producing a few additional resonances. In any case, the effect of these resonances on the thermally-averaged rate coefficient is averaged out. A wider resonance appearing at large internuclear distances (for example, at 5 eV for $R = 1.7$ bohrs) could produce an important contribution to the vibrational excitation cross section at energies above 5 eV. A better treatment of the

vibrational excitation process accounting for electronic resonances is possible and will be developed in a further publication.

Acknowledgments: This work was supported by the National Science Foundation, Grant No. PHY-15-06391. V.K. acknowledges also a support from the Austrian-American Educational Commission.

Author Contributions: Authors contributed equally to this work.

Conflicts of Interest: The authors declare no conflict of interest.

References

1. Roberge, W.; Dalgarno, A. The formation and destruction of HeH^+ in astrophysical plasmas. *Astrophys. J.* **1982**, *255*, 489–496.
2. Dabrowski, I.; Herzberg, G. The predicted infrared spectrum of HeH^+ and its possible astrophysical importance. *Trans. N. Y. Acad. Sci.* **1977**, *38*, 14–25.
3. Black, J. Molecules in planetary nebulae. *Astrophys. J.* **1978**, *222*, 125–131.
4. Flower, D.; Roueff, E. On the formation and destruction of HeH^+ in gaseous nebulae and the associated infra-red emission line spectrum. *Astron. Astrophys.* **1979**, *72*, 361–366.
5. Lepp, S.; Stancil, P.; Dalgarno, A. Atomic and molecular processes in the early Universe. *J. Phys. B At. Mol. Opt. Phys.* **2002**, *35*, R57.
6. Zygelman, B.; Dalgarno, A. The radiative association of He^+ and H. *Astrophys. J.* **1990**, *365*, 239–240.
7. Kraemer, W.; Špirko, V.; Juřek, M. Formation of HeH^+ by radiative association of He^+ + H. An advanced ab initio study. *Chem. Phys. Lett.* **1995**, *236*, 177–183.
8. Strömholm, C.; Semaniak, J.; Rosén, S.; Danared, H.; Datz, S.; van der Zande, W.; Larsson, M. Dissociative recombination and dissociative excitation of $^4HeH^+$: Absolute cross sections and mechanisms. *Phys. Rev. A* **1996**, *54*, 3086–3094.
9. Tanabe, T.; Katayama, I.; Ono, S.; Chida, K.; Watanabe, T.; Arakaki, Y.; Haruyama, Y.; Saito, M.; Odagiri, T.; Hosono, K.; et al. Dissociative recombination of isotopes with an ultra-cold electron beam from a superconducting electron cooler in a storage ring. *J. Phys. B At. Mol. Opt. Phys.* **1998**, *31*, L297.
10. Larson, Å.; Orel, A. Wave-packet study of the products formed in dissociative recombination of HeH^+. *Phys. Rev. A* **2005**, *72*, 032701.
11. Takagi, H. Theoretical study of the dissociative recombination of HeH^+. *Phys. Rev. A* **2004**, *70*, 022709.
12. Larson, Å.; Nkambule, S.; Ertan, E.; Söder, J.; Orel, A.E. Studies of HeH: DR, RIP, VE, DE, PI, MN, ... *EPJ Web Conf.* **2015**, *84*, 03001.
13. Takagi, H.; Tashiro, M. Study on the dissociative recombination of HeH^+ by multi-channel quantum defect theory. *EPJ Web Conf.* **2015**, *84*, 02002.
14. Jimenez-Serra, I.; Martin-Pintado, J.; Viti, S.; Martin, S.; Rodriguez-Franco, A.; Faure, A.; Tennyson, J. The first measurements of the electron density enhancements expected in C-type shocks. *Astrophys. J. Lett.* **2006**, *650*, L135–L138.
15. Rabadán, I.; Sarpal, B.K.; Tennyson, J. Calculated rotational and vibrational excitation rates for electron-HeH^+ collisions. *Mon. Not. R. Astron. Soc.* **1998**, *299*, 171–175.
16. Tennyson, J. Electron–molecule collision calculations using the R-matrix method. *Phys. Rep.* **2010**, *491*, 29–76.
17. Carr, J.; Galiatsatos, P.; Gorfinkiel, J.; Harvey, A.; Lysaght, M.; Madden, D.; Mašín, Z.; Plummer, M.; Tennyson, J.; Varambhia, H. UKRmol: A low-energy electron-and positron-molecule scattering suite. *Euro. Phys. J. D* **2012**, *66*, 58.
18. Seaton, M.J. Quantum defect theory. *Rep. Prog. Phys.* **1983**, *46*, 167.
19. Greene, C.H.; Jungen, C. Molecular Applications of Quantum Defect Theory. *Adv. At. Mol. Phys.* **1985**, *21*, 51.
20. Aymar, M.; Greene, C.H.; Luc-Koenig, E. Multichannel Rydberg spectroscopy of complex atoms. *Rev. Mod. Phys.* **1996**, *68*, 1015.
21. Tennyson, J.; Brown, D.B.; Munro, J.J.; Rozum, I.; Varambhia, H.N.; Vinci, N. Quantemol-N: An expert system for performing electron molecule collision calculations using the R-matrix method. *J. Phys. Conf. Ser.* **2007**, *86*, 012001.

22. Faure, A.; Gorfinkiel, J.D.; Morgan, L.A.; Tennyson, J. GTOBAS: Fitting continuum functions with Gaussian-type orbitals. *Comput. Phys. Commun.* **2002**, *144*, 224.
23. Kokoouline, V.; Dulieu, O.; Kosloff, R.; Masnou-Seeuws, F. Mapped Fourier methods for long-range molecules: Application to perturbations in the Rb_2 (0_u^+) photoassociation spectrum. *J. Chem. Phys.* **1999**, *110*, 9865–9876.
24. Werner, H.J.; Knowles, P.J.; Lindh, R.; Manby, F.R.; Schütz, M.; Celani, P.; Korona, T.; Lindh, R.; Mitrushenkov, A.; Rauhut, G.; et al. MOLPRO, Version 2008.3, a Package of Ab Initio Programs, 2008.
25. Coxon, J.A.; Hajigeorgiou, P.G. Experimental Born-Oppenheimer Potential for the $X^1\Sigma^+$ Ground State of HeH^+: Comparison with the Ab Initio Potential. *J. Mol. Spectrosc.* **1999**, *193*, 306–318.
26. Stanke, M.; Kędziera, D.; Molski, M.; Bubin, S.; Barysz, M.; Adamowicz, L. Convergence of Experiment and Theory on the Pure Vibrational Spectrum of HeH^+. *Phys. Rev. Lett.* **2006**, *96*, 233002.
27. Jungen, C.; Atabek, O. Rovibronic interactions in the photoabsorption spectrum of molecular hydrogen and deuterium: An application of multichannel quantum defect methods. *J. Chem. Phys.* **1977**, *66*, 5584–5609.
28. Kokoouline, V.; Greene, C.H. Theory of dissociative recombination of D_{3h} triatomic ions applied to H_3^+. *Phys. Rev. Lett.* **2003**, *90*, 133201.